RSC Advances

ROYAL SOCIETY OF CHEMISTRY

www.rsc.org/advances

RSC Advances

RSC Publishing

ARTICLE

Entrapment of radioactive uranium from wastewater by using fungus–Fe_3O_4 bio-nanocomposites

Cite this: DOI: 10.1039/x0xx00000x

La Li[a], Mingze Xu[a], Maksim Chubik[c], Marianna Chubik[c], Alexander Gromov[a,c], Guodong Wei[*b] and Wei Han[*a]

Received 00th March 2015,
Accepted 00th March 2015

DOI: 10.1039/x0xx00000x

www.rsc.org/

Magnetically separable adsorbents with high sorption capacity for nuclear wastewater treatment have been successfully synthesized on the basis of fungus–Fe_3O_4 nanoparticle bio-nanocomposites through a simple co-culture method. Experiments demonstrated that fungus–functionalized Fe_3O_4 nanoparticles can be beneficial for avoiding the phenomenon of aggregation for Fe_3O_4 nanoparticles and effectively separating the adsorbents from the contaminated water after adsorption without sacrificing the performances of magnetic adsorbent Fe_3O_4. Indeed, the bio-nanocomposites with improving the sorption capacity can be attributed to the quasi-monodisperse Fe_3O_4 nanomaterials uniformly grown on the macro-scale fungus body. Furthermore, the promising adsorbents with high biological activity can effectively and synergistically remove the radioactive ions from nuclear wastewater with the saturated sorption capacity up to 171 mg/g for $(UO_2)^{2+}$ ions. The fast adsorption process can guarantee that the polluted water could be recovered within only four hours. Our results clearly indicate that the bio-nanocomposites could be used as the cost-effective radioactive adsorbents.

1. Introduction

Radioactive pollutions caused by the use of radioisotopes, nuclear powerplants, nuclear weapon testing, mining industry and medical research have become a serious problem for the environment and attract increasing attention.[1-5] Uranium is one of the most widely used radioactive elements for civilian nuclear power plants and medical research due to its high radiation energy. However, uranium fission and nuclear reactor accidents usually lead to the significant release of radioactive ions into the water and soil around the world.[6] Radioactive Uranyl $(UO_2)^{2+}$ ions, such as from uranium trioxide or uranyl nitrate and other hexavalent uranium compounds, which are generated during uranium reprocess cycles, have been proved to cause birth defects and immune system damage in animal models.[7-10] More worse, uranyl ions in water are very difficult to degrade, and can be accumulated into the human body through the food chains, leading to a serious threat to health and life. For instance, 2011 Fukushima nuclear accident has not only leaked a large amount of radioactive ions into the local water environment, but also has caused global effects, similar to those caused by the Chernobyl accident.[11-13] Therefore, it is imperative to find a cost-effective adsorbent to remove radioactive ions from the nuclear wastewater.

Currently, diverse synthetic inorganic and organic adsorbents at the nanoscale have drawn worldwide attention for their application in water treatment by the following ways: (1) ion-exchange process, such as titanate fibers,[14] (2) complexation, including titanium nanomaterial,[15] 3D flowerlike structures of iron oxide,[16] hollow nest-like nanostructures of α-Fe_2O_3,[17] Fe_3O_4 nanoparticles,[18] polyacrylamide coated-Fe_3O_4 magnetic composites,[19] and amidoxime-functionalized magnetic materials.[20-22] (3) sorption, for instance: carbon nanotubes,[23] magnetic porous carbon,[24, 25] graphene composites,[26] and polymer based composites.[27] (4) chemical/biochemical reductive precipitation.[28] Among them, iron oxide nanoparticles are recognized as a particularly promising material for water treatment applications due to their higher sorption abilities compared to other metal oxide adsorbents, such as TiO_2 and Al_2O_3. Another advangtage of iron oxide adsorbents is that they can be readily reclaimed from the aqueous media by a simple magnetic separation process. However, the iron oxide nanoparticles can cause the secondary dust pollution in the treated water and at the same time aggregation of iron oxide nanoparticles can reduce their adsorption capability. To overcome the problem of aggregation, finding a carrier as the supports to stabilize the nanoparticles on its body is an ideal way to achieve the high dispersion of nanoparticles. In order to meet the requirements of the supporting frame, the carrier should be abundance, low price, and both high compatibility with iron oxide nanoparticles and high adsorption capability.[29, 30] In particular, recyclable bio-adsorbents, such as fungus, could be regarded as a promising candidate for the supporting platform due to the high adsorption capability for $(UO_2)^{2+}$ ions and weak aggregation of Fe_3O_4 nanoparticles.

In this study, novel magnetically separable adsorbents, namely fungus–Fe_3O_4 bio-nanocomposites, were successfully developed by using a simple co-culture method, which can possess the following merits: 1) The Fe_3O_4 nanoparticles with high dispersibility can be uniformly grown on the macro-scale fungus body, improving the sorption capacity due to the weak aggregation of Fe_3O_4 nanoparticles; 2) The bio-nanocomposites have magnetic and thus can be easily oriented and separated from the treated wastewater under applied magnetic field; 3) The bio-nanocomposites with strong vitality can still remain the biological activity even after feeding them into the nuclear wastewater containing high concentration of radioactive ions. This further reduces the difficulty of separation from the contaminated water after the adsorption of radioactive ions. These advantages are greatly conductive to broad applications of the fungus–Fe_3O_4 bio-nanocomposites as promising nuclear adsorbents in water treatment field.

The synthesis process of bio-nanocomposites together with the reaction between fungus and Fe_3O_4 nanoparticles are shown in Fig. 1. First, spores of black aspergillus were cultivated to the sterilized liquid culture medium in an aseptic bench to obtain fungus. Subsequently, 0.05 g Fe_3O_4 nanoparticles prepared by hydrothermal synthesis were dispersed into the solution containing 0.25 g fungus (dry weight). Then, the solution was placed into an incubator oscillator to form the composites. Finally, the bio-nanocomposites with a deep washing were placed in a vacuum oven and dried at 35 °C for 24 hours.

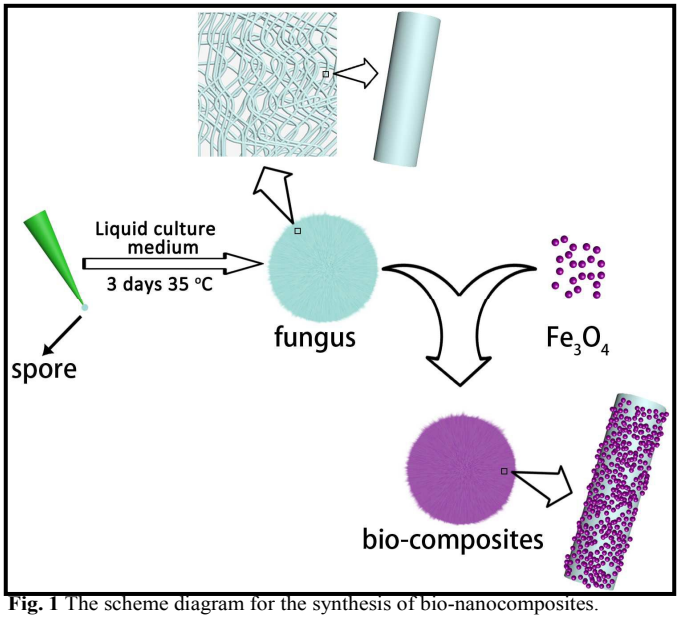

Fig. 1 The scheme diagram for the synthesis of bio-nanocomposites.

2. Experimental section

2.1. The preparation of Fe_3O_4 nanoparticles

In a typical process: First, 30 mL aqueous solution of ferric chloride hexahydrate (0.0833 mol/L) and 30 mL ferrous sulfate heptahydrate solution (0.4583 mol/L) were respectively added to a beaker. Then, 0.65 g sodium dodecyl sulphate was added to the mixture. Subsequently, the solution was placed in a water bath at 65 °C. Aqueous sodium hydroxide was added to the beaker dropwisely until the pH = 12. Then the mixture was aged at constant temperature for 30 minutes. After that, a permanent magnet was used to attract the black powders to the bottom of the beaker. After 20 minutes, the supernatant was removed. The precipitate was washed with deionized water more than three times until the pH of the solution was close to 7, and then washed with ethanol two times. The resulting black powders were kept in an oven at 100 °C for 3 hours.

2.2. The cultivation of fungus

A conventional liquid culture medium for the cultivation of fungus was mixed with beef extract peptone (1.6%), glucose (2%), glycerol (0.5%) and water (95.9%), and then was treated with the traditional high-temperature sterilization method. Spores of black aspergillus were cultivated to the liquid culture medium in an aseptic bench. After growing at 35 ºC for 3 days in a constant temperature shaking incubator, small parts of the mycelia were removed from the culture medium by using a tweezers for the preparation of bio-nanocomposites..

2.3. The preparation of bio-nanocomposites

Firstly, 0.05 g Fe_3O_4 nanoparticles with a BET specific surface area of 147 $m^2 g^{-1}$ were dispersed into the solution containing 0.25 g fungus (dry weight). Subsequently, the solution was placed into an incubator oscillator for 3 days to form the composites. After that, the bio-nanocomposites were washed several times with deionized water to remove the unbinded iron oxide powder from the composites. Finally, the bio-nanocomposites were placed in a vacuum oven and dried at 35 °C for 24 hours for later use.

2.4. The preparation of $(UO_2)^{2+}$ ions solution

Nuclear wastewater solutions with $(UO_2)^{2+}$ concentrations in the range of 20 to 300 mg L^{-1} were prepared for the adsorption experiments by using chemical reagent $UO_2(NO_3)_2 \cdot 6H_2O$ as the uranium source. To obtain the adsorption isotherms, 20 mg of the bio-nanocomposites were added to 20 mL of the solutions with different concentrations of $(UO_2)^{2+}$.

2.5. Characterization

X-ray diffraction (XRD) measurements of the as-prepared product were collected with using a Rigaku D/Max 2550 X-ray diffractometer with Cu Kα irradiation (λ =1.5418 Å) at room temperature. The surface morphology, structure and energy dispersive X-ray analysis were examined with a scanning electron microscopy (SEM) system, using a JEOL JSM-6480LV instrument with an acceleration voltage of 15 kV. Transmission electron microscopy (TEM) experiments were performed by using a JEOL JEM-2100F instrument with an accelerating voltage of 200 kV. The as-prepared fungus–Fe_3O_4 bio-nanocomposites were dispersed in ethanol, and a drop of the homogeneous dispersion was then loaded onto a carbon-coated copper grid and allowed to dry prior to analysis. Fourier transform infrared spectroscopic data (FTIR, AVATAR 370 DTGS) were recorded by using a KBr pellet technique. Finally, the concentration of $(UO_2)^{2+}$ ions in the aqueous solution after adsorption test was analyzed by inductively coupled plasma (ICP).

3. Results and discussion

The structural and morphological characterizations of the fungus, i.e. black aspergillus and fungus–Fe_3O_4 nanoparticle bio-nanocomposites are displayed in Fig. 2. It can be clearly seen that the surface is very smooth for black aspergillus (Fig. 2a) compare with the rough outside surface after attachment of Fe_3O_4 nanoparticles (Fig. 2b). With a closer observation of bio-nanoparticles composites by TEM (Fig. 2c and 2d), the Fe_3O_4 nanoparticles can be randomly distributed on the surface of fungus with an average diameter of 50 nm. In contrast to the morphology of Fe_3O_4 nanoparticles without growing on the fungus (Fig. S1), the aggregation of Fe_3O_4 nanoparticles can be significantly reduced and even eliminated in the bio-nanocomposites by virtue of the dispersive effect of fungus. In addition, according to the selected area electron diffraction pattern (Fig. 2e) of the Fe_3O_4 nanoparticles taken from the area marked in (d), Fe_3O_4 nanoparticles in the bio-composites have the same good crystallinity and structures as the original ones. The (111) and (220) facets of Fe_3O_4 respective corresponding to lattice spacing values of 0.481 nm and 0.297 nm[18] are confirmed by the HRTEM images as presented in Fig. 2f and 2g.

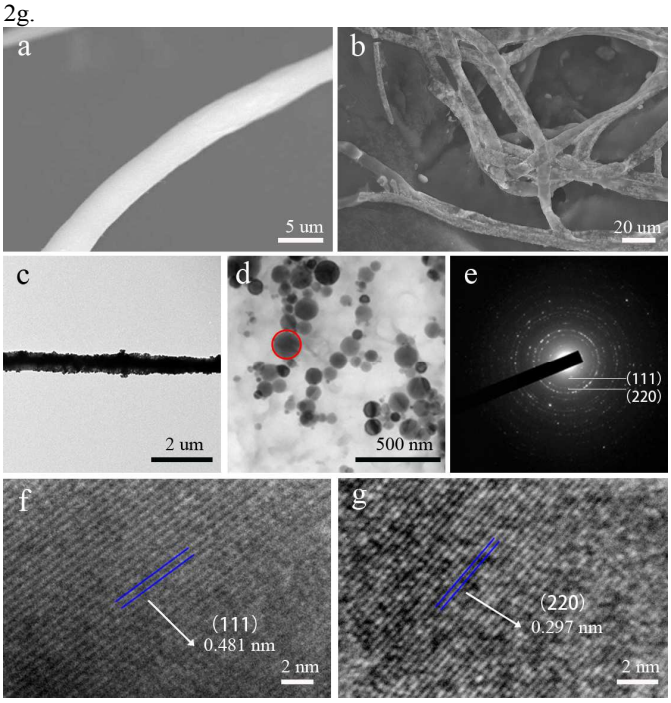

Fig. 2 Typical SEM images of (a) black aspergillus and (b) fungus–Fe_3O_4 composites. (c, d) Typical TEM images at different magnifications of fungus–Fe_3O_4 composites. (e) The SAED pattern of the Fe_3O_4 nanoparticles taken from the area marked in (d). HRTEM images of a single Fe_3O_4 nanoparticle adhered to the fungus, showing the lattice fringes separated by (f) 0.481 for (111) facet and (g) 0.297 nm for (220) facet, respectively.

The crystallization and phase composition of the as-prepared materials were also characterized with using XRD as presented in Fig. 3. It shows that the black aspergillus only has a broad diffraction peak at around 21°. This indicates that it could be a organic material rather than an inorganic material. For Fe_3O_4 nanoparticles, all the diffraction peaks are in good agreement with the peaks of the face-centered cubic (fcc) structure of magnetite. Mössbauer spectra of the Fe_3O_4 nanoparticles shown in Fig. S2 further confirm the high loading content of Fe_3O_4 particles in the bio-composites. For fungus–Fe_3O_4 nanoparticles bio-nanocomposites, considering the fact of high coverage of Fe_3O_4 nanoparticles on the surface of fungus, strong diffraction signals of Fe_3O_4 nanoparticles can be obtained in the XRD curve. In other words, due to the strong XRD signal of inorganic Fe_3O_4 nanoparticles compared with those of the organic fungus, very weak diffraction peak of fungus at ~21° in the bio-composites can not be easy to distinguished in the black curve of Fig. 3

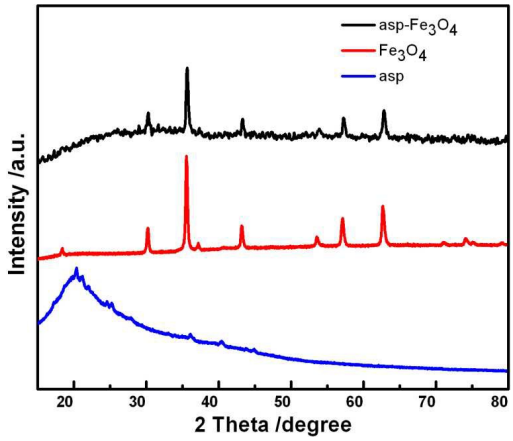

Fig. 3 XRD patterns of black aspergillus (blue curve), Fe_3O_4 nanoparticles (red curve) and fungus–Fe_3O_4 nanoparticles bio-composites (black curve), respectively.

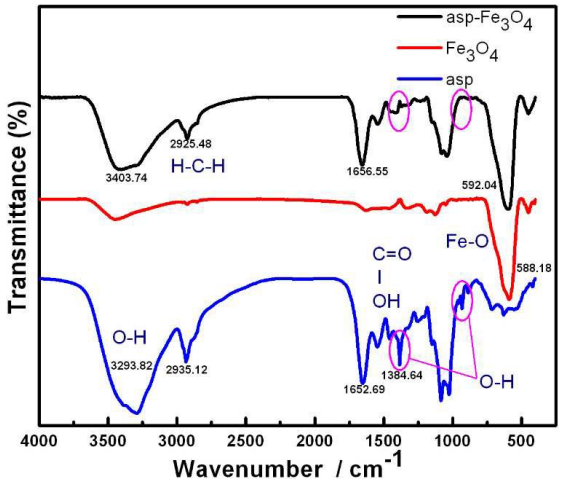

Fig. 4 FTIR spectroscopy of the black aspergillus, Fe_3O_4 nanoparticles and fungus–Fe_3O_4 nanoparticles bio-composites, respectively.

It should be noted that the formed bio-composite structure might be stable enough to use as the nuclear adsorbents. For example, these composites can completely remain their original micro-nano structures even after supersonicated for over 15 min. Therefore, we inferred that the new chemical bonds could be formed between the nanoparticle and fungus during the formation of the fungus-nanoparticle complex. In order to verify the chemical bonds rather than weak physical adsorption, FTIR spectroscopy was used to monitor the changes of the chemical bond during the formation process of fungus–Fe_3O_4 nanoparticle bio-nanocomposites. As shown in Fig. 4 the band of O-H centered at ~1380 cm^{-1} and 920 cm^{-1} is significantly decreased after the conjugation of fungus with Fe_3O_4 nanoparticles, which indicated that certain chemical bonds could be generated between the black aspergillus and the nanoparticles.[31-33] It has been well-demonstrated that the cell wall of fungus is primarily constructed by chitin and glucan,

containing a large number of carboxyl group (the carboxyl group also exists on the surface of Fe_3O_4 nanoparticles). Carboxyl group of chitin on the fungus can be combined with hydrogen atoms of carboxyl group on the surface of Fe_3O_4 nanoparticles when they were placed into an incubator oscillator to form the composites. That is to say the bio-composites can be prepared via the dehydration reaction of the fungus with Fe_3O_4 nanoparticles. The specific reactions between fungus and Fe_3O_4 nanoparticles are displayed in Fig. 5. Thus, the stable bio-composites imply that the interaction between the Fe_3O_4 nanoparticles and fungus may be with the new chemical bonds rather than weak physical adsorption.

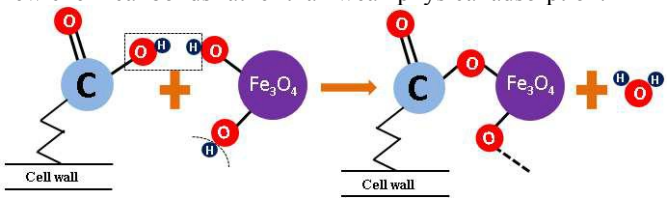

Fig. 5 The scheme diagram for the reaction between fungus and Fe_3O_4 nanoparticles.

Before adsorption experiments were performed, we first measured the Brunauer-Emmett-Teller (BET) surface area of the Fe_3O_4 nanoparticles, which could be an important factor that determines the behaviour of a sorbent. The BET surface area of the Fe_3O_4 nanoparticles is 147 m^2/g and is consistent with previous reports.[18]

The magnetic properties of the Fe_3O_4 nanoparticles and the fungus–Fe_3O_4 nanoparticles bio-composites were investigated at room temperature, respectively. Fig. 6 show their magnetic hysteresis curves measured at room temperature, with the field sweeping from -15000 to 15000 Oe. It can be seen that both samples exhibit a soft magnetic characteristic.[34] From the curves, the saturation magnetization (M_S) was 58.42 emu•g^{-1} (Fe_3O_4 nanoparticles) and 51.18 emu•g^{-1} (bio-composites), respectively. Compared with pure Fe_3O_4 nanoparticles (black curve a), the saturation magnetization of the bio-composites (red curve b) is slightly weakened due to the bio-composites contain a certain amount of non-magnetic organisms. Compared with the M_S value of the 20 nm Fe_3O_4 (57.5 emu •g^{-1}),[35] our bio-composites with the same order of magnitude of M_S can be competitive as the magnetically separable adsorbents. The fast magnetic response of the fungus–Fe_3O_4 nanoparticle bio-composites can be also demonstrated in the insert of Fig. 6. The high magnetic and fast magnetic response of the bio-composites are beneficial for application in nuclear water treatment due to the characteristics of magnetic recycling.

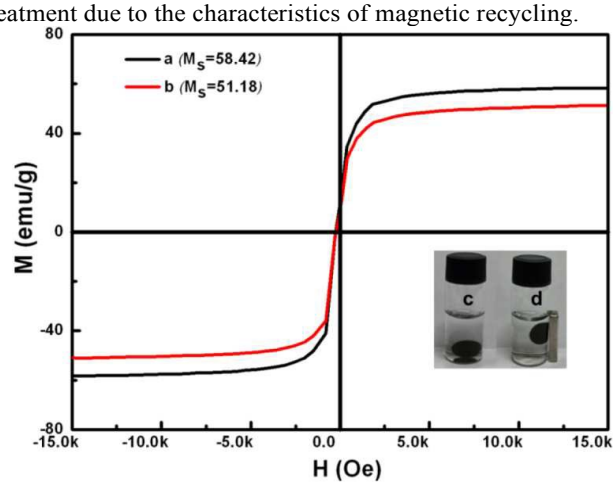

Fig. 6 Room temperature magnetization curves for (a) the Fe_3O_4 nanoparticles and (b) the fungus–Fe_3O_4 nanoparticles bio-composites, respectively. Photographs of magnetite bio-composites dispersion in a vial: (c) without applied magnetic field and (d) with applied magnetic field for only 0.5 min.

Due to the magnetic property and large surface area, these bio-composites with inherent magnetic recycling can be expected to have a good adsorption performance. The uptake of $(UO_2)^{2+}$ ions by the fungus–Fe_3O_4 nanoparticle bio-composites is presented in Fig. 7a. According to the slope, the saturated adsorption capacity can be estimated to be 171 mg/g. It is interesting that the value is much higher than that of only using Fe_3O_4 nanoparticles (110 mg/g) or fungus (63 mg/g, see Fig. S3). The high adsorption capacity for the bio-composites can be attributed to the following facts: 1) Fungus can not only act as a supporting frame, but also can adsorb a certain amount of $(UO_2)^{2+}$ ions (63 mg/g); 2) Fe_3O_4 nanoparticles can grow uniformly on the surface of fungus and thus the bio-composite system can effectively weaken the agglomeration effect of the Fe_3O_4 nanoparticles. In order to fully understand the performances of our adsorbents in the nuclear adsorbent family, the adsorption capacity of our bio-composites and choosing some typical adsorbents with high adsorption capacity for $(UO_2)^{2+}$ removal have been listed in Table 1 for comparison.

In addition to the high adsorption capacity, the promising nuclear adsorbents must have the two following advantages for practical application in the removal of radioactive cations after the nuclear leak: fast absorption time and selective sorption behavior. As shown in Fig. 7b, the adsorbed amount of $(UO_2)^{2+}$ ions reach the absorption equilibrium within only 4 hours, showing an outstanding dynamic advantage. The selective uptake of $(UO_2)^{2+}$ ions by the bio-nanocomposites in the presence of a high concentration of Na^+ was investigated. As shown in Fig. 7b, the co-existed Na^+ in the solution can have negligible effect on the uptake of $(UO_2)^{2+}$ ions for bio-composites. For instance, 82.3% of the $(UO_2)^{2+}$ ions can be removed by the bio-adsorbents, when the molar ratio of U ions to Na^+ ions was as high as 1:20, revealing the high selective sorption behaviour. Moreover, it is found that the pH value of waste water can be changed from acid (4.5~6) to neutral after adsorption experiments. This indicates the bio-composites are also beneficial for restoring the polluted environment.

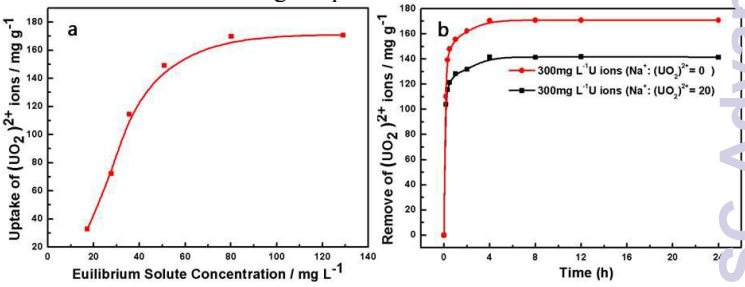

Fig. 7 (a) Removal of $(UO_2)^{2+}$ ions from solutions by bio-nanocomposites. (b) $(UO_2)^{2+}$ adsorption kinetics in 300 mg $L^{-1}(UO_2)^{2+}$ ions with different concentrations of Na^+ as a competitive ion.

Table 1 Comparison of the U sorption capacity of bio-composites with other sorbents.

Sorbents	U capacity, q_m (mg/g)	ref
polyacrylamide coated-Fe_3O_4 magnetic composites	220.9	19
amidoxime-functionalized magnetic	277.3	20

mesoporous silica		
amidoxime-functionalized Fe_3O_4@SiO_2 core–shell magnetic microspheres	105	21
amidoximated magnetite/graphene oxide composites	285	22
fungus–Fe_3O_4 bio-nanocomposites	171	this work

In order to test the stability of our bio-composites during the adsorption process, these biocomposite adsorbents after adsorption experiments have been examined with SEM. Typical SEM images of the bio-nanocomposites after adsorption experiments directly demonstrated that the bio-composite adsorbents can be stable enough to withstand the harsh environment during the sorption process in the high concentration radioactive ions solution due to they still remain their original structure and no Fe_3O_4 nanoparticle particles peeled from the fungus can be found in the solution, as shown in Fig. 8a. The ratio of the adsorbed uranium and Fe in the bio-composites after adsorption is 1.56:1 in Fig. 8b and at the same time the high enrichment of uranium in the final adsorbents can be used to verify the fact that our bio-composites can have a very high adsorption capacity for radioactive ions. Compared with the corresponding SEM image of the bio-nanocomposites after adsorption $(UO_2)^{2+}$, shown in Fig. 8c, the mapping image of element uranium distribution (green dots in Fig. 8d) is in good agreement with the frame of fungus. Obviously, the enrichment of U element in such magnetical adsorbents from wastewater can be beneficent for our recycling process. These properties of high adsorption capacity, fast absorption time, selective sorption behaviour, stable structure together with inherent magnetically recycling demonstrate that the bio-nanocomposites can be regarded as a promising nuclear adsorbent for removal of $(UO_2)^{2+}$ ions from waste water.

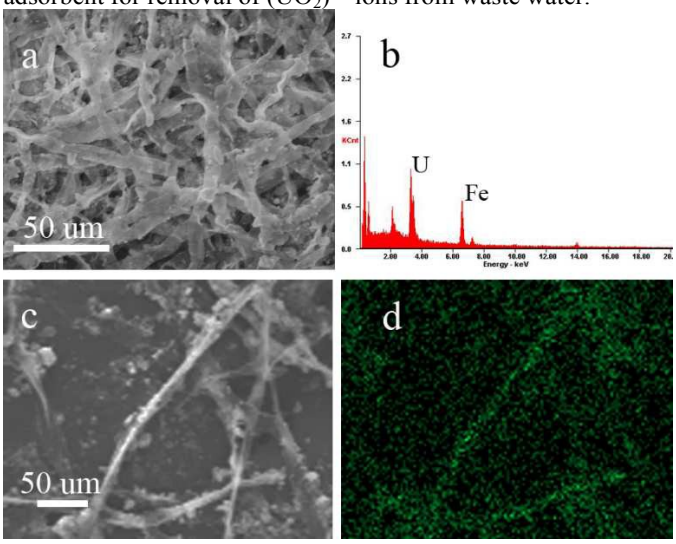

Fig. 8 (a) A typical SEM image of the bio-nanocomposites after adsorption. (b) The EDAX of the bio-nanocomposites after adsorption taken from the area marked in (a). (c) The SEM image of the bio-nanocomposites after adsorption, and its corresponding (d) mapping of element uranium distribution.

4. Conclusions

In summary, we developed a simple environmental-friendly method to synthesize the novel recyclable adsorbent of fungus-Fe_3O_4 bio-nanocomposites. Utilizing the inherent magnetic property of Fe_3O_4 nanoparticles, the bio-nanocomposites can greatly reduce the difficulty of recycling process and avoid the secondary pollution caused by Fe_3O_4 nanoparticlaes. The adsorption tests further demonstrated that the bio-nanocomposites can effectively preconcentrate the trace radioactive ions from nuclear water, with a saturated adsorption capacity of $(UO_2)^{2+}$ as high as 171 mg/g. Obviously, these bio-nanocomposites can be also used to remove other radioactive ions similar to $(UO_2)^{2+}$ ions. It is believed that in the future the novel bio-composite adsorbents will play an important role in the treatment of nuclear waste water.

Acknowledgements

We would like to thank Prof. Jin Wang at the State University of New York at Stony Brook, Prof. Kun Liu at the State Key Laboratory of Supramolecular Structure and Materials of Jilin University for polishing the manuscript and Prof. Fengjun Zhang at Key Lab of Groundwater Resources and Environment Ministry of Education Jilin University for the experimental support. This work was supported by National Key Technology R and D Program (Grant No. 2012BAJ25B10) and National Natural Science Foundation of China (Grant No.41472214).

References

[a] College of Physics, Jilin University, Changchun, 130012, P.R. China.
E-mail: lila206@aliyun.com Fax: +86 (0)43185167869
[b] Tomsk Polytechnical University, Tomsk, 634050, Russia.
[*a] Corresponding author: whan@jlu.edu.cn
[*b] Corresponding author: wgd588@163.com

†Electronic supplementary information (ESI) available: The SEM image and Mössbauer spectra for Fe_3O_4 nanoparticles is shown in supplementary information. See DOI: 10.1039/x0xx00000x

1 M. R. Awual, S. Suzuki, T. Taguchi, H. Shiwaku, Y. Okamoto and T. Yaita, *Chem. Eng. J.*, 2014, **242**, 127-135.
2 N. M. Mubarak, J. N. Sahu, E. C. Abdullah and N. S. Jayakumar, *Sep. Purif. Rev.*, 2014, **43**, 311-338.
3 D. J. Yang, Z. F. Zheng, H. Y. Zhu, H. W. Liu and X. P. Gao, *Adv.Mater.* 2008, **20**, 2777-2781.
4 D. Yang, S. Sarina, H. Zhu, H. Liu, Z. Zheng, M. Xie, S. V. Smith and S. Komarneni, *Angew. Chem. Int. Edit.*, 2011, **50**, 10594-10598.
5 Belgacem, R. Rebiai, H. Hadoun, S. Khemaissia and M. Belmedani, *Environ. Sci. Pollut. Res.*, 2014, **21**, 684-694.
6 S. Sarina, A. Bo, D. Liu, H. Liu, D. Yang, C. Zhou, N. Maes, S. Komarneni and H. Zhu, *Chem. Mater.*, 2014, **26**, 4788-4795.
7 W. Prout, *Soil Sci.*, 1958, **86**, 13-17.
8 L. Wang, A. S. Chen, G. M. Lewis, T. J. Sorg and W. Supply, *Arsenic and Uranium Removal from Drinking Water by Adsorptive Media: US EPA Demonstration Project at Upper Bodfish in Lake Isabella, CA: Interim Evaluation Report*, National Risk Management Research Laboratory, Office of Research and Development, US Environmental Protection Agency, 2008.
9 J. Watson, I. Croudace, P. Warwick, P. James, J. Charnock and D. Ellwood, *Sep. Sci. Technol.*, 2001, **36**, 2571-2607.
10 M. Anke, O. Seeber, R. Muller, U. Schafer and J. Zerull, *Chem Erde-geochem.*, 2009, **69**, 75-90.
11 M. Xu, G. Wei, N. Liu, L. Zhou, C. Fu, M. Chubik, A. Gromov and W. Han, *Nanoscale*, 2014, **6**, 722-725.
12 D. Yang, H. Liu, Z. Zheng, S. Sarina and H. Zhu, *Nanoscale*, 2013, **5**, 2232-2242.
13 D. Yang, H. Liu, L. Liu, S. Sarina, Z. Zheng and H. Zhu, *Nanoscale*, 2013, **5**, 11011-11018.
14 D. Yang, Z. Zheng, H. Liu, H. Zhu, X. Ke, Y. Xu, D. Wu and Y. Sun, *J. Phys. Chem. C*, 2008, **112**, 16275-16280.
15 M. A. Kiser, P. Westerhoff, T. Benn, Y. Wang, J. Perez-Rivera and K. Hristovski, *Environ. Sci. Technol.*, 2009, **43**, 6757-6763.
16 L. S. Zhong, J. S. Hu, H. P. Liang, A. M. Cao, W. G. Song and L. J. Wan, *Adv. Mater.*, 2006, **18**, 2426-2431.

17 Z. Wei, R. Xing, X. Zhang, S. Liu, H. Yu and P. Li, *ACS Appl. Mater. Inter.*, 2013, **5**, 598-604.
18 L. Feng, M. Cao, X. Ma, Y. Zhu and C. Hu, *J. Hazard. Mater.*, 2012, **217-218**, 439-446.
19 W. C. Song, M. C. Liu, R. Hu, X. L. Tan and J. X. Li, *Chem. Eng. J.*, 2014, **246**, 268-276.
20 Y. Zhao, J. Li, S. Zhang and X. Wang, *RSC Adv.*, 2014, **4**, 32710-32717.
21 Y. Zhao, J. Li, L. Zhao, S. Zhang, Y. Huang, X. Wu and X. Wang, *Chem. Eng. J.*, 2014, **235**, 275-283.
22 Y. Zhao, J. Li, S. Zhang, H. Chen and D. Shao, *RSC Adv.*, 2013, **3**, 18952-18959.
23 Pan and B. S. Xing, *Environ. Sci. Technol.*, 2008, **42**, 9005-9013.
24 X. Wang, S. Zhang, J. Li, J. Xu and X. Wang, *Inorg. Chem. Front.*, 2014, **1**, 641-648.
25 S. Zhang, X. Wang, J. Li, T. Wen, J. Xu and X. Wang, *RSC Adv.*, 2014, **4**, 63110-63117.
26 K. C. Kemp, H. Seema, M. Saleh, N. H. Le, K. Mahesh, V. Chandra and K. S. Kim, *Nanoscale*, 2013, **5**, 3149-3171.
27 Y. Huang, J. Li, X. Chen and X. Wang, *RSC Adv.*, 2014, **4**, 62160-62178.
28 L. Liu, W. Liu, X. Zhao, D. Chen, R. Cai, W. Yang, S. Komarneni and D. Yang, *ACS Appl. Mater. Inter.*, 2014, **6**, 16082-16090.
29 J. Wang and C. Chen, *Biotechnol. Adv.*, 2006, **24**, 427-451.
30 H. Y. Zhu, Y. Q. Fu, R. Jiang, J. Yao, L. Xiao and G. M. Zeng, *Bioresource technol.*, 2012, **105**, 24-30.
31 Bosch, D. Serra, C. Prieto, J. Schmitt, D. Naumann and O. Yantorno, *Appl. Microbiol. Biotechnol.*, 2006, **71**, 736-747.
32 V. Shapaval, T. Moretro, H. P. Suso, A. W. Asli, J. Schmitt, D. Lillehaug, H. Martens, U. Bocker and A. Kohler, *J. Biophotonics*, 2010, **3**, 512-521.
33 V. Shapaval, J. Schmitt, T. Moretro, H. P. Suso, I. Skaar, A. W. Asli, D. Lillehaug and A. Kohler, *J. Appl. Microbiol.*, 2013, **114**, 788-796.
34 H. Yang, L. Sun, J. Zhai, H. Li, Y. Zhao and H. Yu, *J. Mater. Chem. A*, 2014, **2**, 326-332.
35 Hui, C. Shen, J. Tian, L. Bao, H. Ding, C. Li, Y. Tian, X. Shi and H. J. Gao, *Nanoscale*, 2011, **3**, 701-705.

